International Journal of Scientific Research in Science and Technology
Print ISSN: 2395-6011 | Online ISSN: 2395-602X (www.ijsrst.com)
doi : https://doi.org/10.32628/IJSRST

Design and Implementation of Neural Network Controller based Modified UIPC for Power Flow Control in grid connected Hybrid Microgrids

Boreddy Sravani[1], Dr. K Siva Kumar[2], M Harish Kumar[3]
M. Tech Student[1], Associate Professor, HoD[2], Assistant Professor[3]
Department of Electrical and Electronics Engineering, SVPCET (Autonomous), Puttur, Karnataka, India

Article Info

Publication Issue
Volume 10, Issue 1
January-February-2023

Page Number
239-252

Article History
Accepted: 10 Jan 2023
Published: 30 Jan 2023

ABSTRACT

In this research work, Design and Implementation of Neural Network Controller based Modified UIPC for Power Flow Control in grid connected Hybrid Microgrids is implemented. In the conventional system, parallel converters are employed for the power conversion process in Hybrid microgrids which consists of AC and DC microgrids. This increases the system complexity and power losses. So, in order to overcome these issues a Modified UIPC is implemented. This UIPC consists of mainly two converters they are line power converter and Bus power converter (BPC). In this BPC is used to regulate the voltage at the DC link Side. A Fuzzy Logic Controller based controlling topology is employed in the BPC as a traditional method. But by employing FLC will imprecise data and has harmonic distortions. In order to overcome these issues this paper proposes a NN Controller based topology. This NN topology will be designed by using the input which reduces the system performance by improving good power quality. The simulation results of this proposed method can be evaluated by using Matlab/Simulink Software.

Keywords : Modified UIPC, Neural Networks, FLC, Power converter, hybrid systems

I. INTRODUCTION

Photovoltaic (PV) frameworks, energy units (FCs), vitality stockpiling frameworks (ESSs), and recently introduced DC loads have grown in popularity over the previous ten years. , Electronic burdens with programmable DC, for example, have entered the conventional force frameworks via DC microgrids [1]. However, AC power assets such as For aggregating both renewable resources and AC/DC loads, a hybrid microgrid structure is the most likely option. This is because the benefits of AC and DC microgrids are combined in this structure. Power exchange control between interconnected AC and DC microgrids in this structure has long been an issue. In this study, UIPC-based solutions are proposed as a better alternative to parallel-connected power converters.., Microgrids are a coordinated half breed framework [4]. Force converters, in fact, connect the AC and DC microgrids. When necessary, this organisation enables

Copyright: © the author(s), publisher and licensee Technoscience Academy. This is an open-access article distributed under the terms of the Creative Commons Attribution Non-Commercial License, which permits unrestricted non-commercial use, distribution, and reproduction in any medium, provided the original work is properly cited

microgrids to trade power... Larger amounts of intensity are commonly traded using force converters. as well as increase consistency [5]. The structure of a typical matrix-associated half-breed microgrid is depicted in Figure 1. In this diagram, the DC microgrid may include PV frameworks, ESSs, and other burdens associated with typical DC transport. [6]. A wind turbine, a diesel generator, and typical AC loads may be included in the AC microgrid [7]. The entire half-and-half microgrid could be linked to the force framework. separated [8]. Interlink power converters (ILCs), as shown in Figure 1, connect the basic transports (joins) of two microgrids.

However, there are some specialised difficulties in resembling power converters in crossover microgrids [8-17]:

Microgrids have unique characteristics such as high voltage levels, stage, recurrence, and force change.

A mixture microgrid can be made up of multiple microgrids. Two alternating current microgrids, for example, and one direct current microgrid. Trading power between microgrids with equal associated ILCs in such an arrangement with various elements is difficult and perplexing due to the voltage magnitude and duration of the basic microgrid transports must be the same in order to avoid flowing current between equal associated ILCs.

- The transferred force between microgrids must be consistently distributed among equal associated ILCs with equivalent force appraisals.

hanges in the framework boundaries, such as line impedance and load variety, have an impact on the force sharing execution of the equal associated ILCs.

Because the flaw in a microgrid is nonlinear, the deficiency current may be distributed inconsistently among ILCs. In this case, the current flowing through the force converters is expected to exceed the apparent current constraints of the force converters, and thus it may be disconnected, resulting in a significant decrease in traded power. As a result, burden concealment or even precariousness may occur in a microgrid...

- The intermittent behaviour of some distributed generation (DG) units in microgrids results in many uncertainties in generated power as well as oscillations in exchanged power between microgrids.

- In AC microgrids, distortions such as harmonics cause a phase difference between ILCs that causes a voltage drop [15].

Power factors of parallel-connected ILCs may differ. This causes oscillations in voltage and power and has an impact on power sharing. performance.

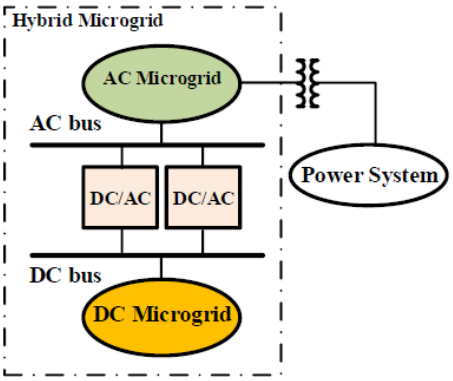

Fig. 1. A typical grid-connected hybrid microgrid

To address the issues mentioned above, numerous procedures and control techniques have been proposed in writing. [12] proposes a multileveled control system for bidirectional equal associated ILCs. The foundation of the control strategy was fixed reference outline (SRF), with no shared term among tomahawks, and was followed by consonant review. This technique has the advantage of being simple to implement because it has been structured..

[13] proposes a hang control-based various levelled control technique in the SRF, with a hang plot serving as the primary control level. On the DC side, the corresponding essential (PI) regulators were used, while on the AC side, the proportional resonant (PR) regulator was used. The primary control level's wave has been modified by the second control level. level control activity, with the utility being connected to the crossover microgrid via the third control level. In this paper, a secure dynamic force control conspire for network-connected crossover microgrids is proposed. [14]. To vary the magnitude of dynamic and receptive

force motions, the technique employs a tunable scalar. [15] demonstrated that voltage imbalance causes force vacillations. As a control technique, controlling the current of each parallelconnected ILC has been proposed. A force converter was used to adjust the sum of all ILC flows. As a result, one of the ILCs was designated as "excessive" and received higher ratings. This raises the price of the control plot..

Similarly, the proposed method is ineffective against consonant bending, and the strategy is incapable of reducing responsive force motions. In [16], a vigorous control plot is intended for power sharing control between two identically associated inverters. The method has used union examination to structure the current inverter regulator. [17] depicts a perfect fragmentary The request regulator was created to share power between two parallel-connected inverters. [18] researchers created cross-breeds. microgrids in demonstrates a decentralised and self-advanced control framework for confined microgrids in accordance with IEEE 1547.4-2011. The control strategy has provided neighbourhood control activities with no correspondence joins, thereby strengthening the strategy. Flexible AC transmission System (FACTS) devices have also been used to control power flow in alternating current Frameworks for transmission. UIPC is used in this paper to control both the traded power between microgrids and the fundamental framework in a cross breed microgrid. Realities devices have been used in a wide range of force control applications with a variety of control structures.. [20] used the bound together force stream regulator (UPFC) to improve voltage stability. Furthermore, using hereditary calculation, the optimal proportion of UPFCs has been determined. [21] used the between line power stream regulator (IPFC) to control the moved force in a transmission line optimally. [22] authors used static VAr compensators (SVCs) to improve force framework security via monetary investigation. In a transmission line connecting two regions in a force framework, the static simultaneous arrangement compensator (SSSC) has been used. [23]. The SSSC has been persuasive in the exchange of power control between two territories. The UIPC was first introduced in [24]. It is an improved version of the conventional IPC (interphase power regulator) that employs force converters rather than stage moving transformers in each stage. The UIPC's suitability for power stream control has been demonstrated in 24].

This paper focuses on a small-scaled modified UIPC for In a mixed microgrid scenario, control Power was exchanged between microgrids and the primary network. The following are the main commitments of this work:

The UIPC is proposed to control the traded power between micro grids rather than using equal associated power converters, which have a variety of control issues [8-17]. microgrids. as well as the fundamental network in a half-and-half microgrid. The standard UIPC structure, which uses three force converters in each stage, is modified so that power trade control between AC-DC microgrids is accomplished with fewer intensity converters.

- Controlling the UIPC with a DC microgrid associated with its DC transport would be difficult because the microgrid elements in a cross breed microgrid are not exactly the same as the ordinary force framework elements. This paper addresses this issue, and another NDO-MS-SMC-based control technique for the BPC's DC side is introduced. As a result, the focus of this investigation is on using the Controlling the UIPC with a DC microgrid linked to its DC transport would be difficult due to the fact that the microgrid elements in a cross breed microgrid are not identical to the ordinary force framework elements. This paper addresses this problem and introduces a new NDO-MS-SMC-based control technique for the BPC's DC side. As a result, the emphasis of this research is on using.

The UIPC outperforms traditional equal associated power converters in the following ways:

Control of traded power between microgrids without imposing lumbering constraints such as equivalent

voltage extents, stages, and so on, which are typically required to connect the ILCs in equal intervals..

- The UIPC, as illustrated in [24], can undeniably limit the flaw current without the need for an additional force converter, as illustrated in [15]. When compared to control techniques such as the quick force control plot, which has traditionally been used for equal associated ILCs, this component makes the connection more reliable, cost-effective, and less complicated.

- As shown in [24], the UIPC can undeniably limit the flaw current without the use of an additional force converter, as shown in [15]. This component makes the connection more reliable, cost-effective, and less complicated when compared to control techniques such as the quick force control plot, which has traditionally been used for equal associated ILCs.

The DC microgrid's DC and AC transport voltages can be controlled by the UIPC. The use of ordinary equal associated ILCs was not used to grant this trademark.

A modified form of the UIPC is used in this work to connect half and half microgrids, achieving all of the previously mentioned highlights. The following is how the rest of this work is organised: The modified UIPC is shown in Section II. Segment III introduces a new aggravation eyewitness based powerful different surface sliding mode control procedure for determining the vacillations of the altered UIPC's normal DC transport voltage. The reproduction results, as well as the correlation contextual analyses, are depicted in Section IV. Section V completes the work.

II. PROPOSED UIPC BASED STRUCTURE OF HYBRID MICROGRID AND DYNAMIC MODELING

The proposed UIPC-focused hybrid microgrid topology is described in this section. This section also contains The modified UIPC's dynamic model. The hybrid microgrid under consideration is shown in Figure 2. As previously stated, the A grid-connected hybrid microgrid is made up of one AC microgrid and one DC microgrid.. that are linked together by the UIPC. The AC microgrid is made up of a diesel generator and related AC and DC components. A PV system, a battery, and AC and DC loads are all part of the DC microgrid. The loads, PV system, and battery are all linked to a single direct current bus (DC link).).

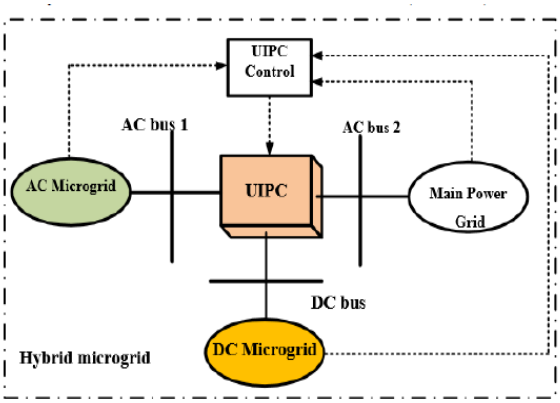

Fig. 2. Interconnection of AC-DC microgrids in grid-connected hybrid microgrid using UIPC

A. Conventional UIPC

[24] describes and illustrates the UIPC's per-phase model. In this structure, voltage source converters replaced the phase-moving IPC transformers (VSCs). Along these lines, two alternating current transports, such as...1 and...2, are used., are linked in each stage by three VSCs, such as...1,...2,...3,... VSC1 and VSC2 are stage shifting converters, while VSC3 is a voltage controlling converter. The arrangement voltage is injected by VSC1, which operates inductively. T1 After connecting the transformer to the line....., VSC2 operates in capacitive mode, injecting the arrangement voltage..... to the line via transformer T2. VSC3, for example, is the third VSC.controls the AC voltage and is connected to one of the AC transports, in this case..1, via transformer T3. A constant capacitor provides DC transport for all VSCs, which are connected in parallel. As a result, the dynamic forces for each VSC are provided by the voltage at which the DC connection is made..... As a result, the power traded between the two alternating current transports would be managed via VSC1 and VSC2 stage edge control. [24] provides more nuance.

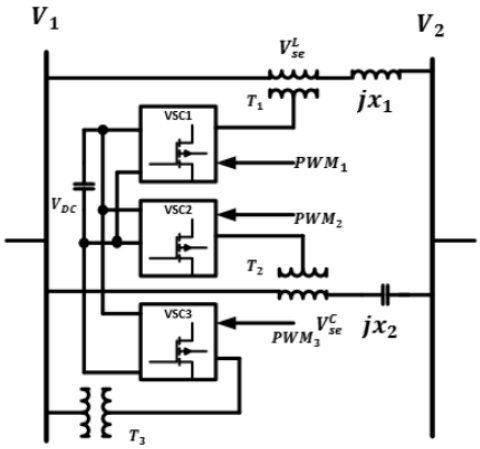

Fig. 3. Conventional structure of UIPC; each phase implements three power converters [24]

B. Proposed structure of UIPC

First, the traditional UIPC topology described in the preceding subsection will be altered. In the following subsection, the modified UIPC's control strategy will be demonstrated. The traditional UIPC structure, as depicted in Fig. 3, has the following flaws: - Because each phase uses three VSCs, connecting three phases of AC buses requires nine VCSs and nine power transformers, making the topology extremely expensive..

- Each phase's DC links have all of their VSCs connected in parallel. However, as described in [12, 25], the VSCs with common DC links are prone to oscillating the common DC link voltage when the output powers of the VSCs change or when there is a disturbance on the system model, such as a change in a system parameter. Voltage fluctuations in the DC link are a major source of concern in VSCs that share a DC link[24] makes no mention of it.

To overcome the aforementioned barriers, the modified UIPC model depicted in Fig. 4 is proposed. Each phase, as shown, only has one power converter, designated as LPCj.

Line numbers are j1,2,3. The series voltage Vse se=Vser+jVsei is injected to each line These power converters are powered by transformers Tj, where Vser and Vsei represent real and imaginary components of the injected series voltage.. The line ZLj=RLj+jXLj is the equation for calculating impedance. In general, the injected series voltage is a controlled voltage source of the following general form:

The voltage amplitude and phase coefficients are denoted by KA and KP, respectively. In fact, the voltage amplitude coefficient KA is pulse dependent, and the phase coefficient KP is usually equal to 1, and se is usually equal to 2The switches S1 and S2 are anti-parallel thyristors coordinated by the injected voltage phase angle via the control system. Only one of these switches is active at any given time, depending on the sign of the phase angle. When the voltage phase coefficient KP is set to +1, The UIPC goes into inductive mode (IM), and both S1 and S2 light up. When the phase coefficient KP is -1, the same thing happens., the UIPC enters capacitive mode (CM), with S1 turned off and S2 turned on. As a result, the power Exchanged between the two AC buses, V1 and V2, can be controlled. It's also worth noting that there is only one BPC in Fig. 4 for all phases. The DC microgrid's DC bus is then linked to the BPC. The BPC is also linked to one of the AC buses (a weaker AC bus, i.e. an AC microgrid bus), in this case V1, in order to control the AC voltage and exchange power with the DC microgrid.. via transformer TBPC. Figure 5 depicts a vector diagram of the system voltages with the proposed UIPC's injected voltage included. This diagram may result in; $\varphi_{se}^L = \varphi_1 + \alpha_1$ $\varphi_{se}^C = \varphi_2 + \alpha_2$

These angles are computed using the UIPC's various operation modes, namely IM and CM. When If the UIPC is in IM or CM mode, seLand seCare the voltage phase angle at the transmission line's midpoint.

The power exchanged between the two AC buses is described by the complex power flow concept. is as follows [26].

$$S = V_2\left(\frac{V_1 - V_2}{Z_L}\right)^* = (V_2\cos\delta_2 + jV_2\sin\delta_2)\frac{(V_1\cos\delta_1 + jV_1\sin\delta_1 - V_2\cos\delta_2 - jV_2\sin\delta_2)^*}{R_{L1} - jX_{L1}} \quad (4)$$

where V1 and V2 have phase angles of 1 and 2. Equation (4) can be written as follows after some mathematical fiddling.

$$P = \frac{R_{L1}V_1V_2(\cos\delta_1\cos\delta_2+\sin\delta_1\sin\delta_2+R_{L1}V_2^2)-X_{L1}V_1V_2(\cos\delta_1\sin\delta_2-\sin\delta_1\cos\delta_2)}{{R_{L1}}^2+{X_{L1}}^2} (5)$$

$$Q = \frac{R_{L1}V_1V_2(\cos\delta_1\sin\delta_2-\sin\delta_1\cos\delta_2)+X_{L1}V_1V_2(\cos\delta_1\cos\delta_2+\sin\delta_1\sin\delta_2+X_{L1}V_2^2)}{{R_{L1}}^2+{X_{L1}}^2} (6)$$

:

In microgrids, $RL1 \gg XL1$ and we get:

$$P = \frac{V_1V_2(\cos\delta_1\cos\delta_2+\sin\delta_1\sin\delta_2+R_{L1}V_2^2)}{R_{L1}} = \frac{V_1V_2}{R_{L1}}(\cos(\delta_1-\delta_2)+R_{L1}V_2^2) \quad (7)$$

$$Q = \frac{V_1V_2(\cos\delta_1\sin\delta_2-\sin\delta_1\cos\delta_2)}{R_{L1}} = \frac{V_1V_2}{R_{L1}}\sin(\delta_2-\delta_1) \quad (8)$$

As a result, The magnitudes of the transferred active power are controlled by the magnitudes of the AC bus voltages, whereas the phase angle difference is controlled by the phase angle difference. The proposed UIPC regulates the magnitude and phase angle difference of the voltage, implying that the active and reactive powers exchanged between two AC buses are regulated. are easily controlled. We obtain the Kirchhoff Voltage Law and Fig. 6 to evaluate the effects of the UIPC's injected voltage.:

$$V_1\angle\delta_1 - V_2\angle\delta_2 = (R_{L1}+jX_{L1})I + V_{se}\angle\varphi_{se} \quad (9)$$

$$= (R_{L1}+jX_{L1})\frac{P-jQ}{V_2^r-jV_2^i} + \left(V_{se}^r+jV_{se}^i\right) =$$

$$\left(\frac{V_2^r(R_{L1}P+X_{L1}Q)+(X_{L1}P-R_{L1}Q)}{(V_2^r)^2+(V_2^i)^2}+V_{se}^r\right)$$

$$+j\left(\frac{V_2^r(X_{L1}P-R_{L1}Q)+(R_{L1}P+X_{L1}Q)}{(V_2^r)^2+(V_2^i)^2}+V_{se}^i\right)$$

In the microgrids, $XL1P \cong RL1Q$ and we get:

$$V_1\angle\delta_1 - V_2\angle\delta_2 = \left(\frac{V_2^r(R_{L1}P+X_{L1}Q)}{(V_2^r)^2+(V_2^i)^2}+V_{se}^r\right)+jV_{se}^i \quad (10)$$

Also, $RL1P \gg XL1Q$ and we have:

$$V_1\angle\delta_1 - V_2\angle\delta_2 = \left(\frac{V_2^r+V_{se}^r\left((V_2^r)^2+(V_2^i)^2\right)}{(V_2^r)^2+(V_2^i)^2}\right)+jV_{se}^i \quad (11)$$

The power exchanged between the DC link and the AC link (..1) can be calculated using the power balance equation:

$$V_{DC}I_{DC}^{UIPC} = \frac{3}{2}V_1^d i_1^d$$

Using the power balance equation, we can calculate the power exchanged between the DC link and the AC link (...1).

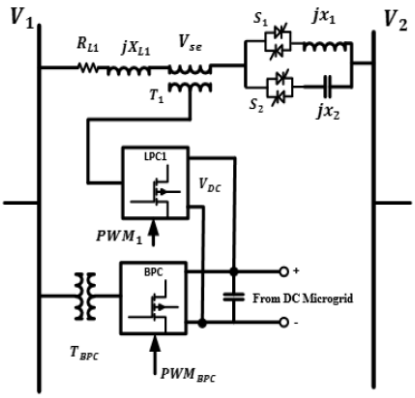

Fig. 4. UIPC topology proposed (each phase implements only one power converter, named as LPC)

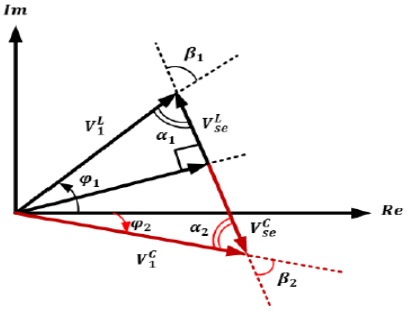

Fig. 5. Voltages when the proposed UIPC is involved

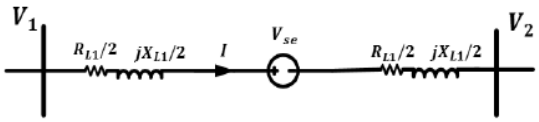

Figure 6 depicts a model of each phase of the system taking into account the proposed UIPC's injected voltage.

The proposed per-stage geography of the cross breed microgrid's UIPC-based interconnected microgrids is depicted in Fig. 7. This figure also depicts the general control structure of the proposed UIPC. There are two subsystems in the control framework: Series VSC control and DC connect control based on NDO-MS-SMC. The Series VSC Control subsystem regulates the infused voltage as well as the switches S1 and S2, and its design incorporates an ideal H-based fluffy rationale regulator. The control subsystem is depicted in the following section. The SMC-based DC connect Control subsystem is in charge of balancing normal DC interface voltage fluctuations and is dependent on another aggravation observer-based hearty various surface sliding mode control system. This control

structure technique is shown in the diagram. diagram below. g area.

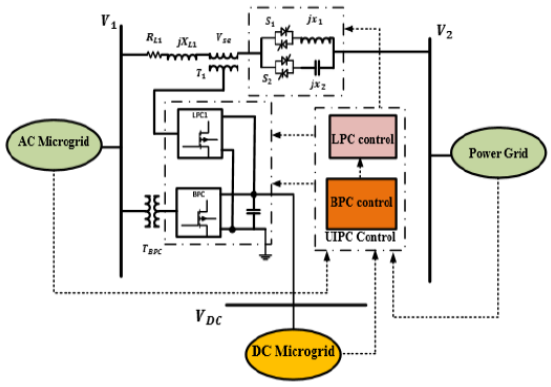

Figure 7: AC-DC microgrid interconnection per-phase model using UIPC and UIPC control system.

To summariseBased on NDO-MS-SMC, series VSC control and DC connect control are provided. The Series VSC Control subsystem regulates the infused voltage as well as the switches S1 and S2, and it is designed with an ideal H-based fluffy logic regulator. The following section illustrates the control subsystem. The SMC-based DC connect Control subsystem is responsible for balancing normal DC interface voltage fluctuations and is reliant on another aggravation observer-based hearty various surface sliding mode control system. The diagram illustrates this control structure technique.

The DC microgrid provides the DC interface voltage. Using this component, the UIPC can connect the AC and DC microgrids.

- -To reduce errors, an ideal fluffy rationale regulator is used in the LPCs' control structure. C.

Proposed control strategy for LPCs

-As shown in Fig. 7, the proposed control scheme for the proposed UIPC structure includes two control subsystems: LPCs control methodology and SMC-based BPC control plot. These control subsystems also collaborate on control. The proposed control method for each LPC at each stage is shown in Figure 8. The voltage and current of the infused arrangement are calculated and scaled. These scaled signs' significant components are then obtained using a bandpass channel. MATLAB [27] is used to determine the boundaries of this channel (move work) as follows:

- As shown in the following section, the voltage peaks and valleys of the DC interface are dampened using an unsettling influence eyewitness-based powerful different surface sliding mode control technique..

$$T_f = \frac{190.10s}{s^2+190.10s+145321}$$

After that, the filtered signals' root mean square (rms) values are computed. The proposed optimal fuzzy logic controller takes into account the injected voltage error (FLC). The injected voltage's phase is determined. PLLs are used. Based on the sign of this phase, which is KP in Equation (1), it is concluded that the UIPC operates in either IM or CM mode.. As a result, the proper phase shift is applied: +2 for IM mode and 2 for CM mode. Furthermore, the switches S1 and S2 are enabled or disabled depending on the operation mode.. The optimal FLC is created using the H filtering design procedure, which the authors of this work have fully described and validated in [28As shown in Fig. 8, a DC link voltage signal is fed to the control systems of all LPCs for coordination. The error signal is then displayed. fed into an optimal FLC. As a result, these signals are used to generate the reference control signal for the PWM unit. The modulator controls the amplitude of the injected voltage (via KA). PWM scheme, as shown in Equation.

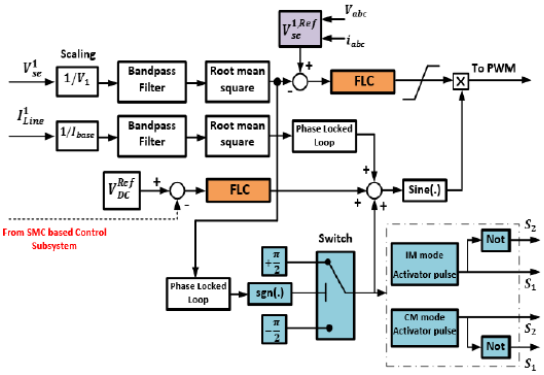

Fig. 8. LPC control strategy proposed

III. PROPOSED NDO MULTIPLE SURFACE SMC BASED DC LINK VOLTAGE CONTROL OF UIPC

The LPC and BPC DC links are connected in parallel to the DC microgrid's common DC bus. As previously stated, changes in the output active power of power

converters, loads, or the PV system would cause the DC link voltage in the DC microgrid to be unstable. As a result, in this section, a new NDO-MS-SMC is used to control the proposed UIPC's DC link voltage.....

A. Structure of proposed control scheme

Fig. 9 depicts the proposed BPC control scheme. As previously stated, the BPC is responsible for regulating the DC link, so The proposed NDO-MS-SMC strategy is used on the BPC. The proposed control scheme is divided into three parts, as shown in Fig. 9. The voltage control loop is the first loop. The current control loop is ranked second, and the NDO is ranked third. The NDO is in charge of calculating the DC microgrid's uncertainties and power changes. The NDO also serves as a timer. reference signal. compensation unit and current control loop. The voltage control loop makes use of optimal proportional controlsIn conjunction with feedforward,.-integral (PI) controllers are used. To compensate for the constitutional delay, a power disturbance is introduced into the dynamics of the The current control loop and the proposed disturbance observer. The genetic algorithm is used to optimise the PI in both current and voltage control loops. controllers (GA).

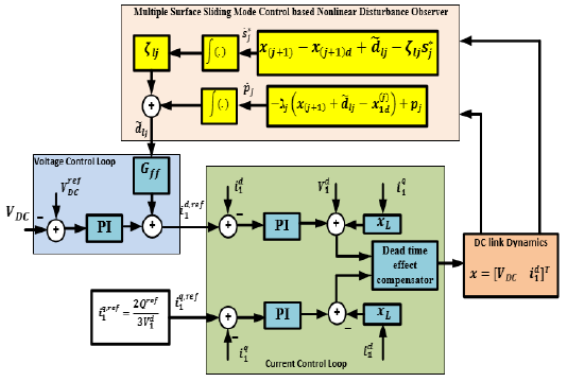

Fig. 9. Control of DC link of BPC based on new NDO-MS-SMC strategy

B. Dynamic model of nominal system

To begin, the nominal model will be used to extract the dynamic equations of the BPC's common DC link without using any parametric uncertainty. Using Kirchhoff Current Law, we get:

$$C\frac{dV_{DC}}{dt} = -I_{DC}^{UIPC} + I_{dist} \qquad (14)$$

The disturbance current is Idist=IDCPV+IESS+IL, where IDCPV is the PV system output DC current, IESS is the energy storage system (ESS) current (for example, a battery), and IL is the lumped DC loads current.

In dq-frame, the BPC model is expressed as follows [29]:

$$\begin{cases} V_o^d = V_1^d + L\left(\frac{di_1^{dt}}{dt}\right) + \omega L i_1^q + i_1^d R \\ V_0^q = L\left(\frac{di_1^q}{dt}\right) - \omega L i_1^d + i_1^q R \end{cases} \qquad (15)$$

Where Vo and V1 are the output AC voltage of the BPC and the AC bus to which it is connected, respectively, is the angular frequency in rad/s, and L and R are the inductance and resistance of the BPC's output filter.

As a result of Equations (12), (14), and (15), we obtain:

$$\begin{cases} \frac{dV_{DC}}{dt} = -\frac{3V_1^d i_1^d}{2CV_{DC}} + \frac{1}{C} I_{dist} \\ \frac{di_1^d}{dt} = \frac{V_o^d - V_1^d}{L} - \omega i_1^q - \frac{R}{L} i_1^d \end{cases}$$

Equation (17) indicates a system with nonlinear terms. This is the nominal model of the system.

C. Dynamic model of perturbed system

The following uncertainties are taken into account for the DC link capacitance C, the disturbance current Id, and the inductance L:

$$\frac{1}{C} = \frac{1}{\bar{C}(1+\rho_C\theta_C)} = \frac{1}{\bar{C}} - \frac{\rho_C}{\bar{C}}\theta_C(1+\rho_C\theta_C)^{-1} \qquad (18)$$

$$\frac{1}{L} = \frac{1}{\bar{L}(1+\rho_L\theta_L)} = \frac{1}{\bar{L}} - \frac{\rho_L}{\bar{L}}\theta_L(1+\rho_L\theta_L)^{-1} \qquad (19)$$

$$I_{dist} = \bar{I}_{dist}\left(1+\rho_{I_{dist}}\theta_{I_{dist}}\right) \qquad (20)$$

where C, L, and Idist represent the nominal values of C, L, and Idist, respectively, and C, L, and Idistrepresent the likely perturbations on these parameters, which are random numbers ranging from -1 to +1.

When we introduce these perturbed parameters into the nominal system (17), we obtain:

$$\dot{x_1} = \left(\frac{1}{\bar{c}} - \frac{\rho_c}{\bar{c}}\theta_c(1+\rho_c\theta_c)^{-1}\right)\left(-\frac{3V_1^d x_2}{2x_1}\right) + \left(\frac{1}{\bar{c}} - \frac{\rho_c}{\bar{c}}\theta_c(1+\rho_c\theta_c)^{-1}\right)\left(\bar{I}_{dist}(1+\rho_{I_{dist}}\theta_{I_{dist}})\right) \quad (21)$$
$$= -\frac{3V_1^d x_2}{2\bar{c}x_1} + \frac{\bar{I}_{dist}}{\bar{c}} + \left(\frac{3V_1^d x_2}{2x_1}\right)\rho_c\theta_c(1+\rho_c\theta_c)^{-1} + \frac{\bar{I}_{dist}}{\bar{c}}\rho_{I_{dist}}\theta_{I_{dist}} - \frac{\bar{I}_{dist}}{\bar{c}}\rho_c\theta_c(1+\rho_c\theta_c)^{-1}(1+\rho_{I_{dist}}\theta_{I_{dist}})$$

$$\dot{x_2} = \left(\frac{1}{\bar{L}} - \frac{\rho_L}{\bar{L}}\theta_L(1+\rho_L L)^{-1}\right)(-Rx_2 + u - V_1^d) - \omega i_1^q \quad (22)$$
$$= \frac{R}{\bar{L}}x_2 + \frac{u}{\bar{L}} - \frac{V_1^d}{\bar{L}} - \omega i_1^q + \frac{\rho_L\theta_L}{\bar{L}}(Rx_2 - u + V_1^d)(1+\rho_L\theta_L)^{-1}$$

D. Design of NDO-MS-SMC

The proposed NDO-MS-SMC, shown in Fig. 9, is designed in this subsection by performing the following steps:

Step 1: Determine the standard form of the perturbed system model: To do so, rewrite Equations (21) and (22) with the following disturbance parameters:

$$d_1(x,t) = \frac{\bar{I}_{dist}}{\bar{c}} + \left(\frac{3V_1^d x_2}{2x_1}\right)\rho_c\theta_c(1+\rho_c\theta_c)^{-1} + \frac{\bar{I}_{dist}}{\bar{c}}\rho_{I_{dist}}\theta_{I_{dist}} - \frac{\bar{I}_{dist}}{\bar{c}}\rho_c\theta_c(1+\rho_c\theta_c)^{-1}(1+\rho_{I_{dist}}\theta_{I_{dist}}) \quad (23)$$

$$d_2(x,u,t) = -\omega i_1^q + \frac{\rho_L\theta_L}{\bar{L}}(Rx_2 - u + V_1^d)(1+\rho_L\theta_L)^{-1} \quad (24)$$

Nonlinear control terminology [30] defines d1(x,t) as matched uncertainty and d2(x,u,t) as unmatched uncertainty. As a result, the system is written in the following general standard form:

$$\dot{x}_n = a(x,t) + b(x,t)u(t) + d_n(x,u,t)$$

where, b=1$\bar{L}$. The disturbance in (25) is continuous

Step 2. Define the multiple surface sliding surfaces, as follows [30]:

$$s_j^* = s_j - s_j(0)e^{-\beta_j t}$$
$$s_j = x_j - x_{jd}$$

where is a positive constant value and xjd represents the desired state trajectory. The goal is to bring each sliding surface sj to zero, resulting in xjxjd. We have the following as a result of obtaining the derivative of the first sliding surfaces:

$$\dot{s}_1^* = \dot{s}_1 + s_1(0)\beta_1 e^{-\beta_1 t} = s_2 + x_{2d} + d_{l1} - \dot{x}_{1d}$$

The estimation error is defined as follows:

$$e_{d_{lj}} = d_{lj} - \tilde{d}_{lj}$$

Step 3. Actual design control law: Up to this point, the virtual control inputs have been designed; they are x1d,2d. To stabilise the uncertain system, the following actual control input is proposed (25):

$$u = -\frac{1}{b(x,t)}\left(a(x,t) + \tilde{d}_{ln} - x_{1d}^{(n)} + \zeta_{ln}s_n^* + \zeta_s sat(s_n^*)\right)$$

Therefore;

$$u = -\bar{L}\left(a(x,t) + \tilde{d}_{l2} - \ddot{x}_{1d} + \zeta_{l2}s_2^* + \zeta_s sat(s_2^*)\right)$$

where, $\zeta l2$ is a linear gain, ζs is the switching gain and the hyperbolic tangent function is approximately equal to:

$$sat(s_2^*) = \begin{cases} sgn(s_2^*) & , \ if\ |s_2^*| > \varrho \\ \frac{s_2^*}{\varrho} & , \ if\ |s_2^*| \le \varrho \end{cases}$$

where, ϱ is a small positive constant. Substituting (32) in (29), the dynamics of the sliding surface $s2*$ is:

$$\dot{s}_2^* = -\zeta_{l2}s_2^* - \zeta_s sat(s_2^*)$$

When obtaining the derivatives of the disturbances in the design procedure, the discrete control part was excluded and did not appear in the derived equations. This is because the designed control signal for the SMC-based controller has two components: the equivalent control energy and the control signal itself. ueqand a discrete part ud that is added to the obtained control signal to improve its resistance to disturbances. It should be noted that when designing the controller, the goal is to obtain the equivalent control energy law ueq based on the Lyapunov energy function. To make the resulting signal more robust, the discrete term ud is manually added to the control law. As a result, the control law's time derivative exists during the period. design process. Please see for further information. [33].

Step 4. Obtaining the disturbance observer dynamics: The NDO aims to estimates the disturbance $\tilde{d}li$ as follows:

$$\begin{cases} \tilde{d}_{lj} = p_j + \lambda_j s_j^* \\ \dot{p}_j = -\lambda_j\left(s_{(j+1)} + x_{(j+1)d} + \tilde{d}_{lj} - x_{1d}^{(j)}\right) \end{cases} \quad -(35)$$

where, pj and λj are a dummy variable and gains of the observer, respectively. Calculating the derivative of $\tilde{d}\ lj$ we get:

$$\tilde{d}_{lj}^{(1)} = \dot{p}_j + \lambda_j\dot{s}_j^* = -\lambda_j\left(s_{(j+1)} + x_{(j+1)d} + \tilde{d}_{lj} - x_{1d}^{(j)}\right) + \lambda_j\left(s_{(j+1)} + x_{(j+1)d} + d_{lj} - x_{1d}^{(j)}\right) = \lambda_j(d_{lj} - \tilde{d}_{lj}) = \lambda_j e_{d_{lj}} \quad (36)$$

and;

$$\|\dot{d}_l\| \le \gamma \quad (37)$$

Step 5. Stability proof: The Lyapunov function is defined as:

$$V_1(e_{d_l}) = e_{d_l}{}^T P e_{d_l}$$

Calculating the derivative of Lyapunov function and using Equations (34)-(36) we get:

$\dot{V}_1 = e_{d_l}{}^T(D^TP + PD)e_{d_l} + 2e_{d_l}{}^TP\dot{d}_l \leq -e_{d_l}{}^TQe_{d_l} + 2\|e_{d_l}\|.\|P\|.\|\dot{d}_l\|$

where, $D = diag[\lambda \quad \lambda]$ Q is a positive arbitrary matrix, and P is a positive matrix such that the following constraint is satisfied.

$$D^TP + PD = -Q \tag{40}$$

Analytically:

$$P = \begin{bmatrix} P_{11} & P_{12} \\ P_{12}^T & P_{22} \end{bmatrix} \tag{41}$$

and we have:

$$\begin{bmatrix} \lambda_1 & 0 \\ 0 & \lambda_2 \end{bmatrix}\begin{bmatrix} P_{11} & P_{12} \\ P_{12}^T & P_{22} \end{bmatrix} + \begin{bmatrix} P_{11} & P_{12} \\ P_{12}^T & P_{22} \end{bmatrix}\begin{bmatrix} \lambda_1 & 0 \\ 0 & \lambda_2 \end{bmatrix} = -Q \tag{42}$$

Therefore, considering Q as an identical matrix, and using (30) and (35)-(37), e_{d_l} will be bounded by;

$$\|e_{d_l}\| \leq \lambda_l \tag{43}$$

where;

$$\lambda_l = \frac{2\|P\|\gamma}{\lambda_m} \tag{44}$$

and the system is robustly stable.

IV. NEURAL NETWORK

A neural network is a network of neurons, or more recently, a synthetic neural network consisting of artificial neurons or nodes.. [1] As a result, a neural A network can be biological or artificial. or an artificial neural network used to solve artificial intelligence-related problems (AI). The connections between biological neurons are represented by weights. A positive value denotes an excitatory connection, whereas a negative value denotes a receptive a negative value represents an inhibitory connection. All inputs are weighted and then added together. A linear The name given to this activity is defined as a combination. Finally, An activation function controls the amplitude of the output. An acceptable output range, for example, is typically between 0 and 1, but it could also be between 1 and 1. These fictitious networks can be trained using a dataset and used for predictive modelling, adaptive control, and other applications. Self-learning can occur as a result of experience within networks that can draw conclusions from a complex and seemingly unrelated set of data..

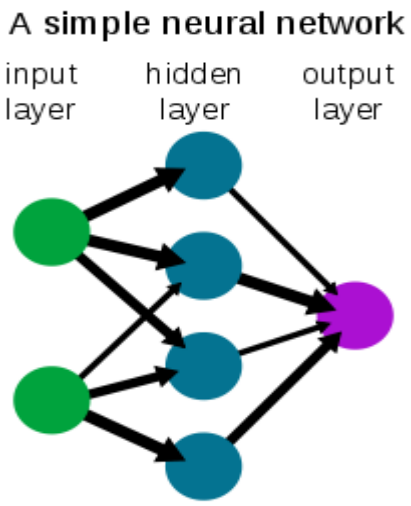

Fig. 10 Simplified view of a feed-forward artificial neural network

Artificial intelligence:

A neural system (NN), also known as a fake neural system (ANN) or a mimicked neural system (SNN), is an interconnected collection of regular or fake neurons that uses a scientific or computational model for data preparation based on a connectionistic approach to calculation. A lot of the time, an ANN is a versatile framework that changes its structure depending on whether data is coming from outside or inside the system..

In simpler terms, neural systems display non-linear factual information or are dynamic. instruments. They can be used to display complex relationships between information sources and outputs or to discover patterns in data. A forgery neural system consists of a system of basic preparing components (fake neurons) that can exhibit complex global behaviour, which is controlled by the associations between the handling components and component boundaries. Warren McCulloch, a neurophysiologist, and Walter Pitts, a rationalist, first proposed fake neurons in 1943 while working together at the University of Chicago..

The repetitive Hopfield organise is an old-fashioned type of phoney neural system. Alan Turing appears to

have first proposed the concept of a neural system in his 1948 paper Intelligent Machinery, which referred to them as "B-type chaotic machines."".

The usefulness of fake neural system models lies in their ability to gather and use information from perceptions. Unaided neural systems can likewise be used to learn information portrayals that capture the exceptional qualities of information appropriation, for example, see the Boltzmann machine (1983), and more recently, profound learning calculations, which can verifiably gain proficiency with the dissemination capacity of the observed information. In applications, learning in neural systems is especially useful. where the unpredictability of the information or task makes manual planning of such capacities impractical.

Applications:

- Neural systems can be used in a variety of fields. The tasks to which counterfeit neural systems are generally applied will fall into the following general classes:
- Function estimation or relapse examination, including time expectation and display.
- Classification, which includes example and grouping recognition, oddity recognition, and successive dynamic.
- Data processing, such as sifting, grouping, dazzle signal partitioning, and pressure.

ANN applications include nonlinear framework identification and control (vehicle control, process control), game-playing and dynamic (backgammon, chess, dashing), design acknowledgment (radar frameworks, face ID, object acknowledgment), grouping acknowledgment (motion, discourse, transcribed content acknowledgment), clinical conclusion, monetary applications, information mining (or information revelation in databases, "KDD"), perception, and email sifting. It is possible, for example, to create a semantic profile of client's inclinations emerging from images prepared for object recognition.

Neuroscience:

The theoretical investigation and computational display of natural neural frameworks are central to the field of hypothetical and computational neuroscience. Because neural frameworks are inextricably linked to cognitive procedures and behaviour, the field is strongly related to psychological and social displaying.

1) The field's goal is to create models of natural neural frameworks in order to understand how organic frameworks work. To gain this understanding, neuroscientists attempt to connect observed natural procedures (information), organically conceivable instruments for neural handling and learning (organic neural system models), and hypotheses (factual learning hypothesis and data hypothesis).

2) **Types of models**

Several models are employed, each with a different level of deliberation and displaying various parts of neural frameworks. They progress from models of transient behaviour of individual neurons to models of neural hardware elements arising from cooperations between singular neurons, and finally to models of behaviour arising from conceptual neural modules communicating with final subsystems. These include long-term and transient pliability models of neural frameworks, as well as their relationship to learning and memory from the individual neuron to the framework level.

V. SIMULATION RESULTS

a. With Conventional controller:

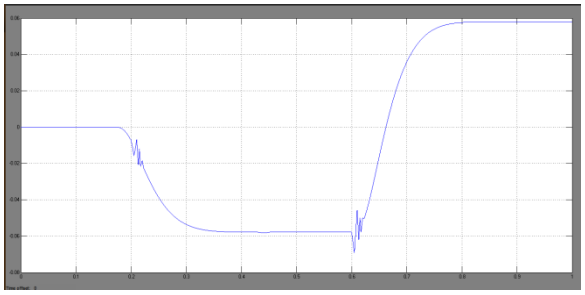

Fig. 11. VSE Series Injected Voltage

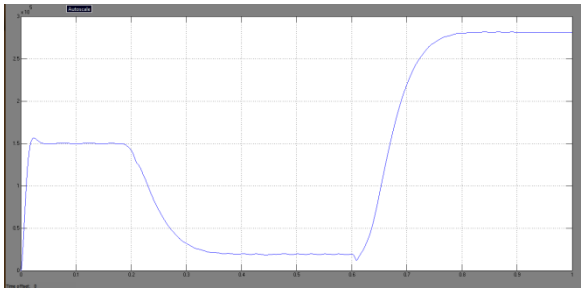

Fig. 12. Pse Injected Power

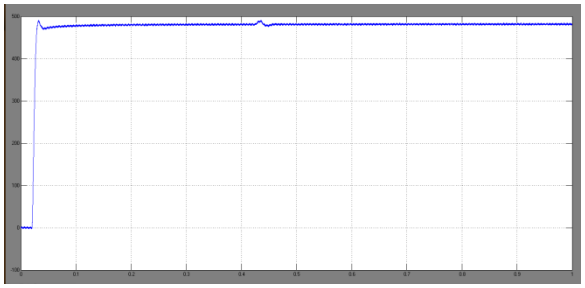

Fig. 13. Dc LINK VOLTAGE

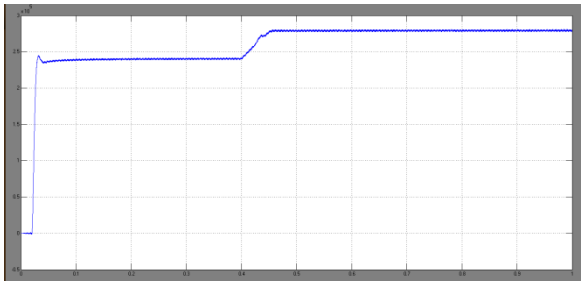

Fig. 14. Active power of DC link when 40 kW is demanded from the AC side

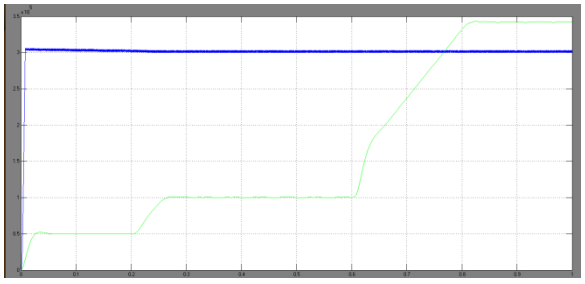

Fig. 15. Generation in each micro grid

b. Simulation results with Neural Nework Controller:

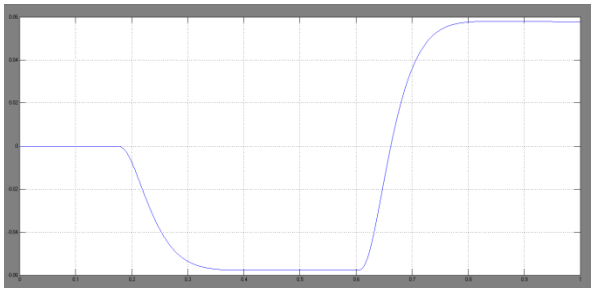

Fig. 16. VSE Series Injected Voltage

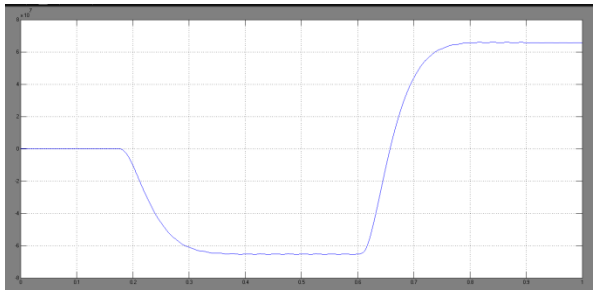

Fig. 17. Pse Injected Power

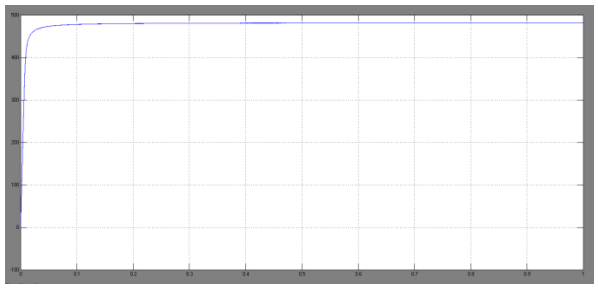

Fig. 18. Dc LINK VOLTAGE

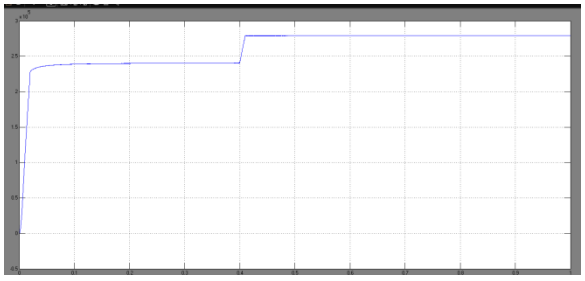

Fig. 19. Active power of DC link when 40 kW is demanded from the AC side

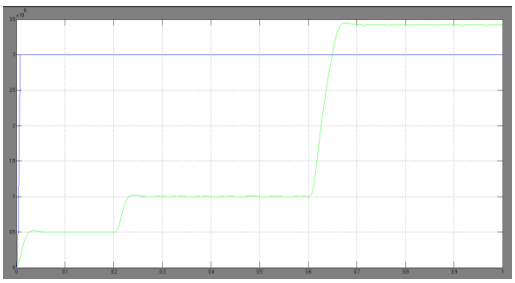

Fig. 20. Generation in each micro grid

VI. CONCLUSION

In this work, the Design and Implementation of Neural Network Controller based Modified UIPC t has been implemented for Power Flow Control in grid-connected Hybrid Microgrids. In the traditional system, parallel converters are used for power conversion in hybrid microgrids, which include both AC and DC microgrids. This has increased the system complexity and power losses. So, in order to overcome these issues a Modified UIPC has been implemented.

This UIPC consists of mainly two converters they are line power converter and Bus power converter (BPC). In this BPC has been used to regulate the voltage at the DC link Side. A Fuzzy Logic Controller based controlling topology has employed in the BPC as a traditional method. But by employing FLC is having imprecise data and has harmonic distortions. In order to overcome these issues the FLC is replaced with NN Controller. This NN topology will be designed by using the input which reduces the system performance by improving good power quality. The simulation results of this proposed method has been evaluated by using Matlab/Simulink Software.

In future smart grids, For aggregating both renewable resources and AC/DC loads, a hybrid microgrid structure is the most likely option. This is because the benefits of AC and DC microgrids are combined in this structure. Power exchange control between interconnected AC and DC microgrids in this structure has long been an issue. As a better option, a UIPC-based solution is proposed. to parallel-connected power converters in this study., which have caused numerous issues. First, a modified UIPC structure is proposed, and then effective control strategies for the modified UIPC are introducedThe simulation results validated both the modified model and the performance of power exchange control between AC and DC microgrids. The system's performance with a Neural Network controller outperforms that of a fuzzy logic controller.

VII. REFERENCES

[1]. Runfan Zhang, Branislav Hredzak, "Distributed Finite-Time Multi-Agent Control for DC Microgrids with Time Delays", IEEE Transactions on Smart Grid, Early Access, 2018.

[2]. Kumar Utkarsh, et al, "Distributed Model-predictive Real-time Optimal Operation of a Network of Smart Microgrids", IEEE Transactions on Smart Grid, Early Access, 2018.

[3]. Haifeng Qiu, et al, " Bi-level Two-stage Robust Optimal Scheduling for AC/DC Hybrid Multi-microgrids", IEEE Transactions on Smart Grid, Early Access, 2018.

[4]. Pengfeng Lin, et al, "A Distributed Control Architecture for Global System Economic Operation in Autonomous Hybrid AC/DC Microgrids", IEEE Transactions on Smart Grid, Early Access, 2018.

[5]. Daniel E. Olivares, et al, "Trends in Microgrid Control", IEEE Transactions on Smart Grid Volume: 5, Issue: 4, pp. 1905 – 1919, 2014.

[6]. Jongwoo Choi, et al, "Robust Control of a Microgrid Energy Storage System using Various Approaches", IEEE Transactions on Smart Grid, Early Access, 2018.

[7]. Huanhai Xin, et al., "A Decentralized Hierarchical Control Structure and Self-Optimizing Control Strategy for F-P Type DGs in Islanded Microgrids", IEEE Transactions on Smart Grid, Volume: 7, Issue: 1, pp. 3 – 5, 2016.

[8]. Priyank Srivastava, Rashmi Pardhi "A Review on Power System Stability and Applications of FACT Devices" International Journal of Engineering Research and Applications, Volume: 3, Issue: 3, pp.879-883, 2013.

[9]. Akanksha Mishra and G.V. Nagesh Kumar, "Congestion Management of Power System with Interline Power Flow Controller Using Disparity Line Utilization Factor and Multi-objective Differential Evolution" CSEE Journal of Power and Energy Systems, Volume: 1, Issue: 3, pp. 76 - 85 2015.

[10]. B. Vijay Kumar, et al., "Optimization of UPFC location and capacity to improve the stability using ABC and GSA algorithm", IEEE, Power and Energy Conference at Illinois (PECI), 2015.

[11]. K.K. Sen, "SSSC-static synchronous series compensator: theory, modeling, and application", IEEE Transactions on Power Delivery, Volume: 13, Issue: 1, pp. 241 - 246 ,1998.

[12].J. Pourhossein, et al., "Unified Interphase Power Controller (UIPC) Modeling and Its Comparison with IPC and UIPFC", IEEE

Cite this article as :

Boreddy Sravani, Dr. K Siva Kumar, M Harish Kumar, "Design and Implementation of Neural Network Controller based Modified UIPC for Power Flow Control in grid connected Hybrid Microgrids", International Journal of Scientific Research in Science and Technology (IJSRST), Online ISSN : 2395-602X, Print ISSN : 2395-6011, Volume 10 Issue 1, pp. 239-252, January-February 2023.
Journal URL : https://ijsrst.com/IJSRST2310126